Available online at www.sciencedirect.com
SCIENCE DIRECT®
Journal of Nuclear Materials 343 (2005) 58–69
journal of nuclear materials
www.elsevier.com/locate/jnucmat

Summary of cavitation erosion investigations for the SNS mercury target

J.R. Haines *, B.W. Riemer, D.K. Felde, J.D. Hunn, S.J. Pawel, C.C. Tsai

Spallation Neutron Source[1], *Oak Ridge National Laboratory, 701 Scarboro Road, MS-6474, Oak Ridge, TN 37830, USA*

Abstract

Intense proton beam-induced heating of the spallation neutron source mercury target will cause pressure spikes that lead to the formation of cavitation bubbles in the mercury. Erosion of the mercury container walls caused by violent collapse of bubbles could potentially limit its service lifetime. In-beam tests for a limited number of pulses (<1000 pulses for each test target) have demonstrated that pitting damage appears to be especially sensitive to beam intensity, surface treatment, and gas injection. Using results of off-line pressure pulse tests conducted for a million cycles or more to scale the results from limited in-beam tests, it is concluded that the mercury target will last at least two weeks at a time-averaged proton beam power level of 1 MW. However, because of remaining uncertainties, it is concluded that further research and development and target design efforts are needed to verify these conclusions and extend the target to higher operating powers and longer lifetimes.

1. Introduction

The mercury target for the spallation neutron source (SNS) must be designed to sustain a time-averaged proton beam power of at least 1 MW deposited in nearly instantaneous (<1 μs) pulses at a 60 Hz repetition rate [1]. One of the most challenging issues associated with applying liquid metals as targets for short-pulse proton beams is withstanding the effects of the intense heating of the liquid metal. Although the resulting temperature rise for a single pulse in SNS is relatively small (~10 K in the peak location for a time-averaged proton beam power level of 2 MW), the rate of temperature rise is enormous (~10^7 K/s) during the very brief event. This heating occurs essentially instantaneously compared with acoustic wave time scales; therefore, the mercury undergoes a large pressure increase.

There are three primary concerns associated with the rapid pressure increase. First, the mercury container must be able to withstand the induced strains. Second, the flow that is required to transport the deposited beam power must not be unduly impeded. Third, the erosion caused by cavitation bubble collapse must be slow enough to yield a reasonable target vessel lifetime. Research and development (R&D) and analyses efforts have demonstrated that the SNS target design adequately addresses the first two items and that they do not present serious performance limitations [2,3]. However, the third issue, namely cavitation-induced erosion of the mercury container, has the potential to seriously limit the service lifetime of the SNS target container. The remainder of this paper summarizes the cavitation

* Corresponding author. Fax: +1 865 574 0966.
E-mail address: hainesjr@ornl.gov (J.R. Haines).
[1] SNS is managed by UT-Battelle, LLC, under contract DE-AC05-00OR22725 for the US Department of Energy.

0022-3115/$ - see front matter © 2005 Elsevier B.V. All rights reserved.
doi:10.1016/j.jnucmat.2004.08.033

erosion studies performed in support of the SNS mercury target.

2. Erosion caused by pressure pulses

2.1. Early cavitation damage tests with mercury

Tests conducted early in the SNS target development program had shown that mercury, with the level of impurities and dissolved gasses expected in the SNS process loop, will cavitate when the tensile pressure reaches a few tenths of a MPa [4,5]. These types of conditions will exist in the target immediately following a proton beam pulse because of the reflection of the initial compression waves as rarefaction waves from the interface between the walls of its container and the surrounding environment. It is well known that cavitation bubble collapse can eventually cause severe damage to surfaces.

Erosion, caused by short-pulse beam deposition, was first observed in the isotope separation on-line device (ISOLDE) molten metal targets [6]. Early SNS cavitation erosion studies conducted using an ultrasonic horn showed that damage with mercury was much more severe than with water at the same power level, but it was not clear how to interpret these results in view of the vastly different pressure and frequency regimes present with the ultrasonic horn tests compared with actual SNS conditions [7].

More recently, a team of researchers at the Japan Atomic Energy Research Institute (JAERI) observed pitting of stainless steel surfaces that were in contact with mercury subjected to large mechanically-induced pressure pulses of the same magnitude as those expected at full-power pulses in SNS [8–10]. In view of the JAERI results, targets used in pulsed proton beam tests before 2001 were examined, but because no pretest inspections had been performed, it was not possible to distinguish between beam-induced pits and other imperfections in the surface of the materials.

Tests conducted during 2001 at the Los Alamos Neutron Science Center's Weapons Neutron Research (LANSCE-WNR) facility were designed to examine whether the pressure pulse phenomenon causes pitting damage to the stainless steel container for the mercury. The WNR beam parameters are summarized in Table 1. Although total energy per pulse was substantially lower than planned for the SNS target, by tailoring the beam size, the maximum energy density (and corresponding induced pressure) in test targets was comparable to that expected in SNS. Using a test target size that was roughly 1/2-scale of SNS, the ratio of the beam cross-sectional area to the target cross-sectional area was also comparable. From the viewpoint of pressure wave transport and considering the beam size and sound speed in mercury, the beam deposition time is sufficiently short to be considered nearly instantaneous in either SNS or the WNR tests.

Table 1
Beam parameters for WNR tests compared to SNS conditions

Parameter	WNR	SNS (@2 MW)
Proton energy (GeV)	0.8	1.0
Protons/pulse (Tera-protons)	28	200
Deposition time (ns)	250	700
Energy deposited per pulse in mercury target (kJ)	2.2	20
Maximum energy deposition density (MJ/m^3)	4–18	12

Test targets consisted of sealed, cylindrically shaped, stainless steel containers filled with mercury. Beam entrance and exit windows were machined flat and highly polished to assist in the identification of any features larger than a few microns that could have been introduced by the test. Scanning electron microscopy (SEM), optical microscopy, and laser profilometry were used to conduct detailed examination of the flange surfaces before and after irradiation.

All four of the diaphragm flanges tested for 200 beam pulses in July 2001 were fabricated from 316LN type stainless steel in the mill-annealed condition. Three of them were used directly, whereas the fourth was first treated with a surface-hardening technique called Kolsterising® (a registered trademark of Bodycote International). A small cluster of large pits, visible to the naked eye, as well as small, randomly distributed pits, were found on the three untreated diaphragms. Only the cluster of large pits was found on the diaphragm treated with the Kolsterising® process [11].

Based on the July 2001 test results, it was concluded that further tests were needed to improve the understanding of this phenomenon and to examine the sensitivity to some material variations and geometric features. Six mercury targets were tested in the December 2001 campaign. Four of the mercury targets used different shapes or different diaphragm materials and were exposed to 200 beam pulses. Most notably, a target with a rectangular cross section was used in an attempt to eliminate the postulated radial focusing of the pressure wave present in the July 2001 tests. Also, diaphragms with increased thickness, intended to reduce the large stresses and strains, were tested. Two mercury targets were tested with only 20 pulses to determine whether future tests might be possible at this reduced fluence level.

Two results from the December 2001 campaign are especially noteworthy. First, a highly cavitation-damage-resistant cobalt alloy (Stellite 6B) was severely pitted. Second, the only surface that survived the tests with no pitting was a thick-walled flange made from 20% cold-worked 316LN SS that had a Kolsterising®

treatment. More detailed discussions of the results of these tests are given in Refs. [12,13].

With cavitation erosion concerns in mind, a set of criteria for deciding whether or not to maintain mercury as the target material was established in April 2002. The criteria were that (1) WNR tests for a target geometry and material combination must show pitting damage that can be scaled from 100 to 200 test pulses to at least 14 days of operation in SNS (7×10^7 beam pulses at 60 Hz) at a time-averaged proton beam power of 1 MW, (2) the high-cycle scaling behavior of "high-pressure pulse" pitting damage must be demonstrated up to at least one million cycles for materials similar to those successfully tested at WNR, and (3) these results had to be available for making a final decision by October 15, 2002.

Results from pitting erosion tests conducted under pulsed-beam conditions (so-called in-beam tests) for up to 1000 pulses and off-line pitting erosion tests using mechanical impulses to create cavitation conditions for a large number of cycles are discussed in Sections 2.1 and 2.2, respectively. The in-beam tests were intended to simulate, as realistically as possible, the damage to be expected in SNS, while the off-line tests were intended to improve understanding of the cavitation erosion phenomenon and provide a means to extrapolate the limited in-beam test results to the large number of cycles needed for an adequate lifetime in SNS.

2.2. Parametric short-pulse beam tests

Twenty-one targets were tested in the June 2002 WNR tests, including variations in target material, geometry, power level, use of gas injection to mitigate the damage, and number of beam pulses (one test ran for 1000 pulses, which represents an order of magnitude increase over the 100 pulses used for the remainder of the tests). Most of the targets used a rectangular geometry as displayed in Fig. 1. Highly polished front (beam entry) and rear (beam exit) end-plates were used as the primary test specimens to measure the degree of pitting damage. As shown in Fig. 2, a highly polished plate was also inserted near the bottom of most targets (located outside the direct beam interaction region) to simulate the small slots used in the SNS target for the target container cooling passage.

Pretest SEM examinations were performed on all of the polished plates. A 5×5 array of micro-indentation marks were applied on each plate to serve as fiducial marks for pretest and post-test images. These marks were centered on the plates and were spaced on an orthogonal grid with a spacing of 5 mm. Images with magnifications of 100× and 400× were recorded at each mark.

The WNR tests were successfully conducted, and the irradiated targets were returned to Oak Ridge National Laboratory (ORNL) for mercury decontamination, followed by post-test SEM examinations. Pitting damage was quantified using image processing software, as described in Ref. [14]. The pitting was characterized primarily using two parameters. The first was simply the fraction of area that was damaged. Data are quoted for the worst SEM image found on a specific plate. The second is the mean depth of erosion (MDE), which was computed for the SEM image with the worst damage. The MDE was calculated by determining the area of each pit on the SEM image with the most pitting damage, calculating an equivalent radius, and assuming that the pit had a conical shape with a depth equal to its radius. The volumes for each pit calculated in this fashion were added together to obtain the total material removed. The MDE is simply this volume of eroded material divided by the area in the SEM image. Based on a limited amount of profilometry measurements, the assumption that the depth of the pits is equal to its radius likely overestimates the pit depth by as much as an order of magnitude.

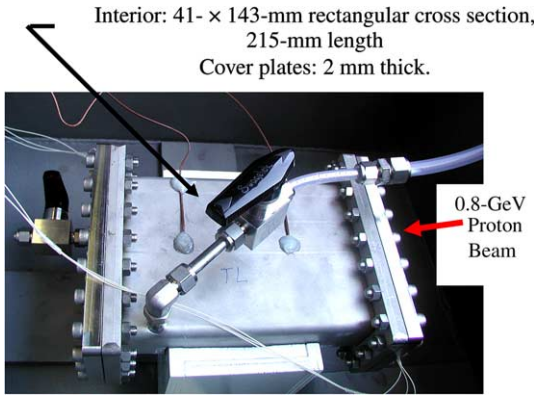

Fig. 1. One of the rectangular targets used in the pitting tests conducted at the WNR facility in June 2002.

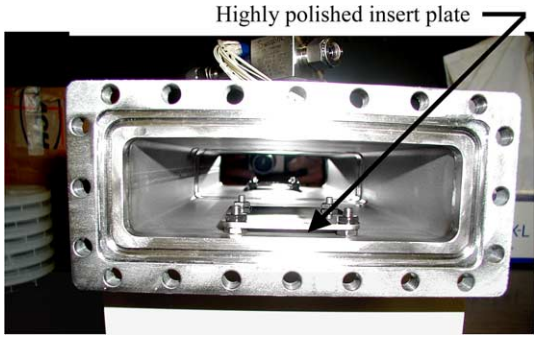

Fig. 2. Inside of rectangular test target showing the insert plate used to simulate the narrow channels that form the SNS target cooling passages.

The reference test case was the rectangular target with 20% cold-worked 316LN SS plates subjected to a beam intensity that gave a volumetric energy deposition equivalent to that for the SNS operating at 2.5 MW with a 60 Hz repetition rate. Pretest and post-test SEM images for the reference case at the location that exhibited the most severe cavitation pitting damage are shown in Fig. 3. The corresponding pitting statistics computed for this case are also included in the figure. In this worst location, almost 5% of the surface is covered with pits and the MDE is 132 nm.

Results for specific surfaces within 14 of the targets are summarized in Table 2. The equivalent time-averaged SNS proton beam power level, as scaled from the peak energy density within the target, is shown in this table to facilitate comparisons.

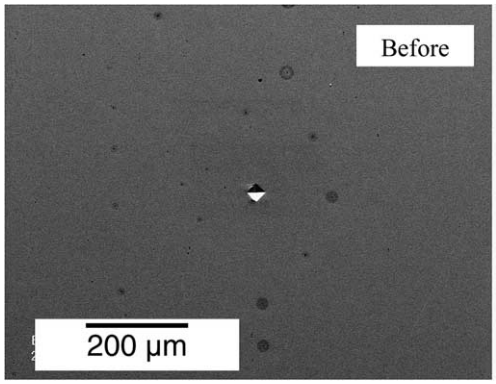

Equivalent SNS Power Level = 2.5 MW

Summary for Image with Worst Damage	
Image # 25665	
Frac Pit Area	0.046
Average Pit Area (μm ^{2})	30.0
Diam of Ave Area Pit (μm)	6.2
Max Area of Pit (μm ^{2})	1600
Diam of Max Pit (μm)	45
Mean Erosion Depth (nm)	132

Fig. 3. SEM images and pitting statistics for the reference case (2.5 MW equivalent power level) from July 2002 WNR tests.

Tests at different energy densities (power levels) show a remarkably strong dependence. Reducing the equivalent power level from 2.5 MW (Target TL) to 1.1 MW (Target TM) reduces the mean depth of erosion by more than an order of magnitude. Data for the lowest power level (Target TH) (0.4 MW equivalent) are unreliable because the number of pits in the worst SEM frame is too small to be statistically significant.

This strong dependence on power/intensity can perhaps be explained as follows. Carpenter and Ruggles have independently noted that the mechanical energy input to the mercury from the "instantaneous" energy deposition from the beam scales as the square of the incident beam energy [15,16]. They argue that both the pressure rise (Δp) and the volume expansion (ΔV) required to relieve the pressure scale directly with beam power deposition (Q). That is,

$$\Delta p \propto Q$$

and

$$\Delta V \propto Q.$$

For pressure rises that are large compared to the static pressure, which is clearly the case in the SNS target situation as well as for the WNR tests, the mechanical energy (E) scales with the product of the pressure rise and volume expansion,

$$E \propto \Delta p \Delta V.$$

Substituting for the pressure rise and volume expansion in terms of beam power deposition gives

$$E \propto Q^2.$$

Thus, the mechanical energy is proportional to the square of the input beam energy.

The relationship between the mechanical energy input to a cavitation damage system and the erosion rate ($\dot{e}$) was explored in early SNS erosion studies using an ultrasonic horn with mercury and a 316LN SS test specimen [7]. As shown in Fig. 4, the erosion rate was shown to have a quadratic dependence on the input mechanical power (note that the data for water erosion at these same power levels showed a linear dependence). That is,

$$\dot{e} \propto E^2$$

Currently, there is no theoretical understanding of why the power dependence is quadratic with mercury and linear with water, this is merely an empirical observation. Nevertheless, taking this empirical result and combining it with the theoretical scaling for the mechanical energy with beam input power, the erosion rate with mercury at 'high proton beam powers' should depend on the input beam power raised to the fourth power,

Table 2
Summary of pitting damage on various surfaces of targets tested at the WNR facility in June 2002

Target	Equivalent SNS power level (MW)	Fraction of area with pits (%)	Mean depth of erosion (nm)
TL – high-power target (*front surface*)	2.5	4.6	132
TM – medium-power target (*front surface*)	1.1	0.3	12
TH – low-power target (*front surface*)	0.4	0.2	4
KILO – 1000 pulse (*front surface*)	2.9	3.6	101
BL – bubble layer (*front surface*)	2.7	0.3	8
K – kolsterized (*front surface*)	3.1	0.03	0.1
EP – electro-polished (*front surface*)	2.8	0.4	4
L – L-shaped (*front surface*)	2.5	2.5	45
N – Nitronic-60 (*front surface*)	2.8	1.4	23
DW1 – H_2O double wall – *front surface 2*	2.2	0.1	5
DW1 – H_2O double wall – *front surface 3*	2.2	2.2	55
DW1 – H_2O double wall – *top surface 3*	2.2	2.0	51
DW2 – Hg double wall – *front surface 1*	2.9	2.9	118
DW2 – Hg double wall – *front surface 2*	2.9	2.0	36
DW2 – Hg double wall – *front surface 3*	2.9	0.6	13
B1 – bubble injection target (*front surface*)	3.4	2.9	65
B2 – tall target (*front surface*)	3.4	7.7	123
B3 – short target (*front surface*)	3.4	0.5	7

All targets, except KILO, exposed to 100 WNR beam pulses.
Note: Surfaces 1, 2, and 3 on double-wall targets (DW1 and DW2) are defined as follows. Surface 1 is in contact with Hg or water in the slot (its other surface is in contact with air). Surface 2 is in contact with Hg or water in the slot (its other surface is in contact with bulk Hg). Surface 3 is in contact with the bulk Hg.

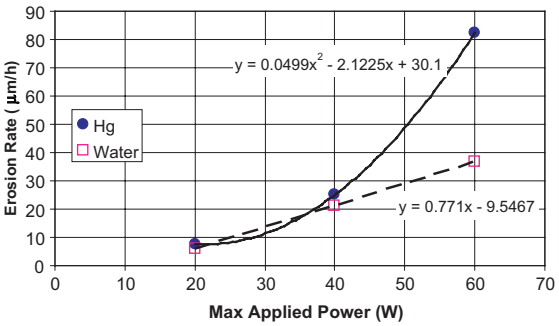

Fig. 4. Dependence of erosion rate on applied power level for ultrasonic horn tests [7].

$\dot{e} \propto Q^4$.

This very strong dependence is roughly consistent with the WNR erosion data, where reducing the power from a 2.5 MW equivalent SNS intensity level to a 1.1 MW equivalent power level reduced the fraction of area damaged from 4.6% to 0.3% and the estimated mean depth of erosion from 132 to 12 nm. Although these data imply that the exponent in a simple power law relationship should be more like 3 rather than 4, they nevertheless confirm a rather strong dependence of erosion on input beam power. It should be noted that the in-beam tests were conducted in the so-called incubation region of cavitation erosion, whereas the power dependence argument given in the previous paragraph applies in the so-called steady-state region of cavitation erosion.

Unlike the power dependence, increasing the number of beam pulses by an order of magnitude (Target KILO) had little effect on the damage, thus indicating a weak dependence on this parameter.

One recommendation of a group of cavitation damage experts convened to review the SNS pitting erosion studies was to test a technique used to acoustically hide naval vessels. A substantial wall of gas bubbles is created around the hull of a ship, creating an impedance barrier that hides the internal mechanical noise of the ship from distant listening devices. A test target (Target BL) was designed to create a curtain of gas bubbles at the beam window in an attempt to hide the window from the pressure pulses created in the mercury. Note that this approach differs from the bubble mitigation technique that will be discussed later in the context of Target B1, which aims to introduce a population of small bubbles dispersed throughout the mercury volume. Comparing the results for Target BL with the reference case (Target TL), it is shown that injecting a layer of gas along the front plate reduced the erosion by more than an order of magnitude. Based on pretest videos, the gas layer was imperfect, covering the beam interaction region of the plate about 80% of the time. Improvements in this

concept could lead to further reductions in the cavitation damage.

The results for the target plate treated with the Kolsterising® process (Target K) showed essentially no pitting damage for the 100-pulse test. This process involves diffusion of carbon in the near-surface material, thereby ensuring that the treatment is graded (i.e., no sudden changes in properties such as those typically encountered with hard coatings). Characterization of the treated layer has shown that although it is about five times harder than annealed 316LN SS, it maintains excellent toughness. The primary uncertainty in using this treatment is whether or not it maintains its properties after significant irradiation. A set of Kolsterised® 316LN SS specimens were recently irradiated to a fluence level of one displacements-per-atom (dpa) in the high flux isotope reactor, but post-irradiation examinations (hardness measurements) are not yet available.

One of the targets (Target EP) used front and rear plates that were electro-polished to a degree sufficient to remove the entire layer of mechanical polishing present on all other specimens. The damage on the electro-polished target was an order of magnitude less than for the reference, mechanically polished case. This difference in erosion could possibly be caused by enhanced damage resistance of the electro-polished surface. Alternatively, it could be more representative of the damage that a surface without the high degree of mechanical polishing would experience.

A noted shortcoming of previous targets was the fact that the real SNS target has no wall opposite the beam window. Pressure waves originating in the front end of the target will propagate down the mercury piping and will not reflect off a wall as they do in test targets. To approximate this lack of a reflecting wall, one test target (referred to as the 'L'-shaped target) was designed with an angled rear wall, which directs waves into an energy-dissipating volume, which has a free surface in contact with helium gas at one atmosphere. This should determine whether the reflections off the rear surface of the test targets are contributing to the damage. As shown in Table 2, the results for the 'L'-shaped target showed little or no advantage compared with the reference case. This could mean that most of the damage occurs in the period immediately following a pulse since one expects that the initial interaction of the front wall with the pressure pulse would be the same for the two targets.

The use of 25% cold-worked Nitronic-60 austenitic stainless steel appeared to reduce the pitting damage by about a factor of three compared with 316LN SS. This is roughly consistent with water cavitation damage literature.

Two rectangular targets were constructed with narrow slots on the front and top surfaces that were filled with either mercury or water to simulate the double-wall structure used to provide cooling for the SNS mercury target container. Three surfaces on the front and three on the top of both targets were polished and examined to characterize pitting damage related to the narrow slot. One target employed mercury in the inter-wall space, while the second used water. The results for the two double-wall targets are at least qualitatively consistent with acoustic wave propagation arguments. The damage on the walls facing the small slot of mercury (target DW2) showed much more damage than the wall facing the bulk mercury. The results for the case with a water-filled slot (target DW1) show little damage on the water side but significant damage on the bulk mercury side.

Although the damage to the insert plates that simulate the walls of the cooling jacket in the SNS target was not quantified, severe damage to this plate was observed. A photograph and SEM image of a small region of the under side (side facing the small slot) of the plate in the TL target is shown in Fig. 5. A line of very large (~50 μm diameter) pits were observed on this plate, and an SEM image near the center of this region is shown in Fig. 6. The pits on this surface appear to be much deeper than those observed on the front plates. Based on these results and the results from the double-wall targets (targets DW1 and DW2), consideration is being given to modifying the SNS target container design to either eliminate this slot or to substitute water to provide the primary cooling for the container wall.

Fig. 5. Photograph showing severe pitting damage along the beam direction on the bottom surface of the 63-mm-wide × 76-mm-long × 3-mm-thick insert plate used in target TL from the June 2002 WNR tests.

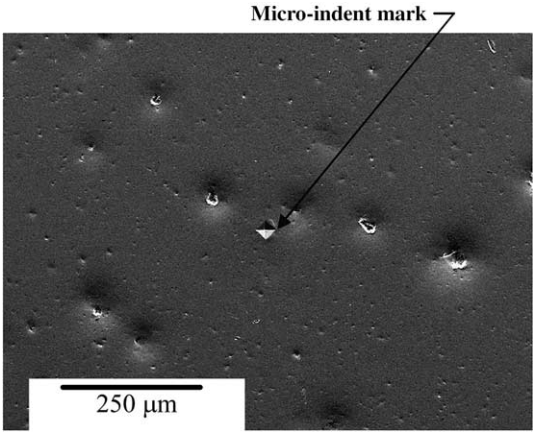

Fig. 6. An SEM image taken in the region with large pits, shown in Fig. 5.

Additional test results, shown in Table 2, for tall, thin targets (targets B1, B2, and B3) showed that injection of bubbles reduced the erosion by about a factor of two compared with an equivalent target without bubbles. The target with bubble injection was in front of the target with no bubbles, resulting in a 20% more intense beam for the target with bubbles. Using the intensity to the fourth power dependence discussed previously, the net benefit for bubble injection is estimated to be about a factor of four. The bubble injection concept can likely be greatly improved as the first operation of the bubble injection system in this configuration occurred moments before the in-beam test.

A target was also included to test a new type of diagnostic to detect the presence of bubbles and to provide information on their size and lifetimes. This target had fiber-optic cables, which terminate at the mercury/stainless steel interface. The concept is to detect bubbles by the changes in reflected laser light from the interface. An additional fiber-optic sensor was employed to detect the presence of bubbles in the bulk fluid. Data taken from this new diagnostic showed promise, but further development work needs to be done to interpret results and obtain detailed quantitative information [17].

2.3. Off-line tests for high cycles

Four off-line test devices have been used to study cavitation erosion with mercury and to help extrapolate the in-beam test data from the limited number of beam pulses to the lifetime goal of 7×10^7. The JAERI team, led by Masatoshi Futakawa [18], built a magnetically driven impact test device called the magnet impact test machine (MIMTM). In addition to continuing to use an ultrasonic horn operating at 20 kHz, the SNS team built a simple drop test device based on the principles of the Split-Hopkinson pressure apparatus used earlier by the JAERI team [19]. A collaborative effort was also established with Robin Cleveland of Boston University to use the university's lithotripter (kidney stone blaster) to create cavitation pits on small specimens.

All of these devices succeeded in creating pitting damage similar to that observed with beam tests, although in some cases it took many more or many fewer pulses to reach an equivalent level of damage. The drop test apparatus and its results are covered more extensively in this paper, since the drop test is not well documented elsewhere, whereas the MIMTM and ultrasonic horn test have been discussed elsewhere [18,20,21]. Although the lithotripter device appeared to also simulate the erosion behavior, it was not pursued beyond the initial stages because of resource and time limitations.

A schematic drawing of ORNL's drop test device is shown in Fig. 7. The 0.3-m-long, 16-mm-diameter striker bar was dropped from a fixed height for each pulse. The striker bar impacts the 0.9-m-long input bar that transmits the approximately one-dimensional pressure wave to a 10-mm-long mercury region that is in contact with the output bar. Samples made from 316 type stainless steel with a diameter of 16 mm and length of 10 mm are threaded onto the ends of the input (upper position) and output (lower position) bars in contact with mercury. Both of the samples were removed periodically to weigh and examine surface damage, either with a digital camera or with an SEM.

Photographs showing the damage of the upper specimen in the drop test apparatus at various numbers of cycles up to 920,000 drops are shown in Fig. 8 for a drop height of 250 mm. The fraction of area pitted is shown in

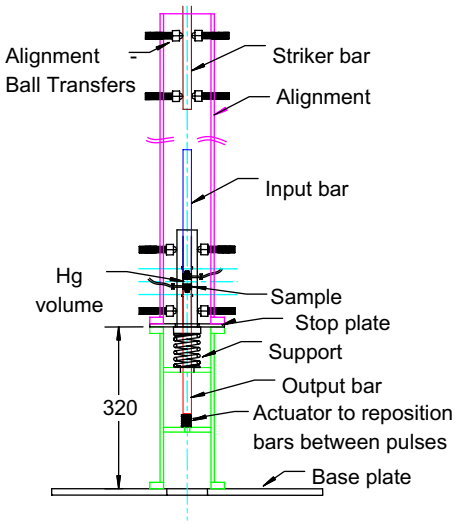

Fig. 7. Schematic drawing of the ORNL drop test apparatus used to study cavitation erosion with high-pressure pulses in mercury.

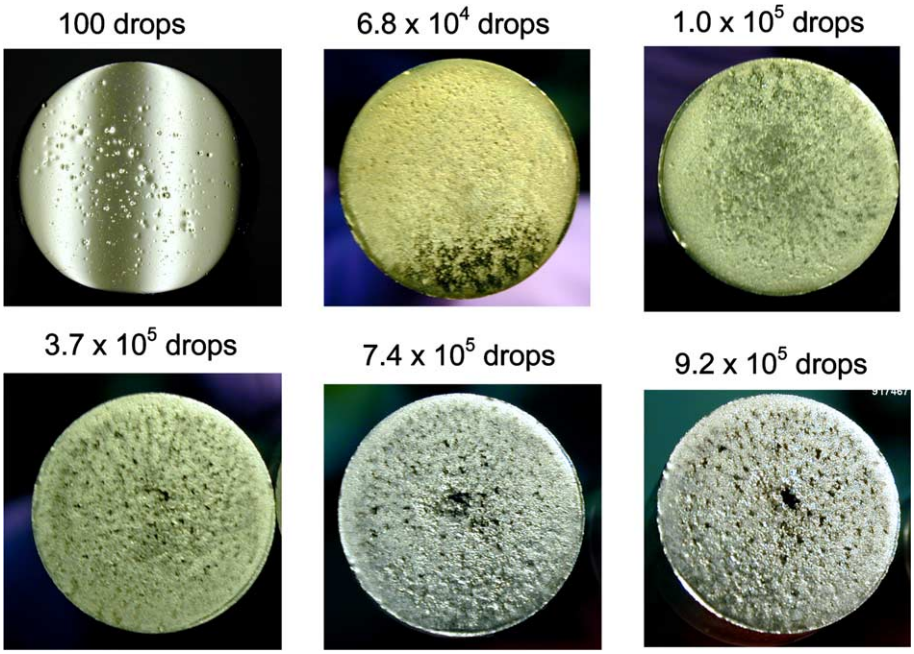

Fig. 8. Photographs showing the progression of pitting damage for a drop test specimen (upper sample position) up to almost one million cycles.

Table 3 for the drop test at two heights, compared with the beam test results for power levels equivalent to 2.5 and 1.1 MW. The pitting damage for the 250-mm drop height is even more severe than the 2.5-MW equivalent proton beam case. Unfortunately, the drop height for conducting most of the tests (250 mm) had to be selected before obtaining the beam test results, so the drop test results were obtained in a more severe regime than that found for the in-beam tests.

Nevertheless, as shown in Fig. 9, the erosion characteristics for the drop test device follow the typical cavitation erosion behavior, displaying a so-called incubation period, where the surface becomes pitted with only minor loss of material, followed by a 'steady-state' phase where bulk erosion occurs. The MDE values plotted in Fig. 9 are based on weight loss measurements. Erosion during the steady-state phase appears to follow a N^{α} dependence, where α is slightly greater than one. Data for cycles less than 10^5 are not shown since weight losses were negligible in this region.

SEM images of the surface of a drop test specimen (upper position) are shown in Figs. 10–13 over the range from 100 to 100,000 cycles. Individual pits can be identified in the images for 100 and 1000 cycles. About 6.1% of the total surface area is covered with pits at 100 cycles, and this fraction increases to 37% at 1000 cycles. After 10,000 cycles, the surface is nearly completely covered with pits and many pits have coalesced. The surface is completely roughened at 100,000 cycles, and as shown in Fig. 9, this number of cycles corresponds roughly to the point where bulk erosion of material becomes significant (i.e., the boundary between the incubation region and the steady-state erosion region).

A final noteworthy observation from the drop test studies is that the damage appears to scale with the square of the input energy. The data displayed in Table 3 show that doubling the energy input by increasing the drop height from 125 to 250 mm increased the fraction of the surface area pitted by nearly a factor of four. This same dependence of the erosion on input mechanical energy was discussed earlier for the ultrasonic horn device.

The ultrasonic horn, which operates at a frequency of 20 kHz, provides erosion data for a relatively large number of cycles in a short period of time; however, it operates at significantly lower pressure pulse intensity than

Table 3
Comparison of pitting damage for ORNL drop tests compared with the WNR beam tests

Test specimen	Fraction of area with pits (%)
250-mm drop	6.1
WNR-2.5-MW equivalent	4.6
125-mm drop	1.8
WNR-1.1 MW equivalent	0.25

Results shown for 100 pulses in all cases.

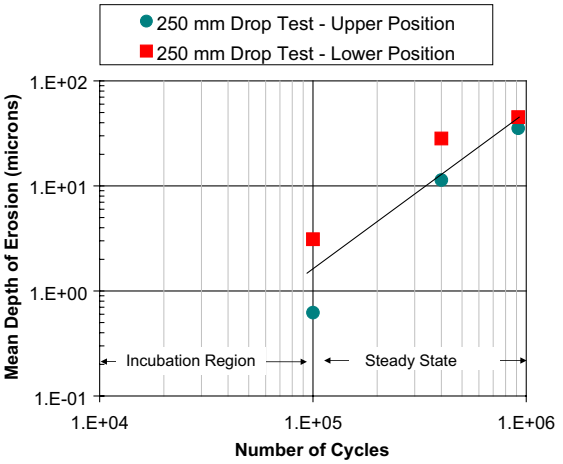

Fig. 9. Mean depth of erosion for drop tests from a height of 250 mm.

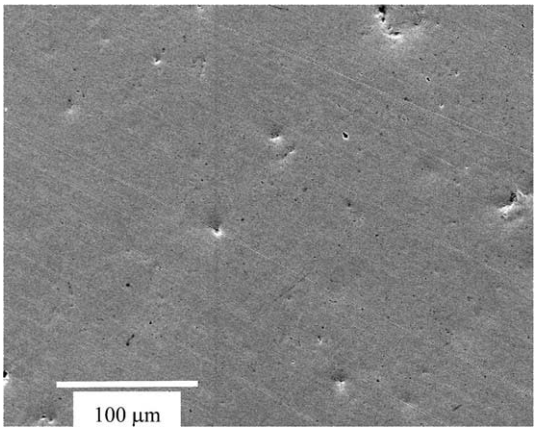

Fig. 10. Micrograph of drop test sample (upper position) after 100 pulses.

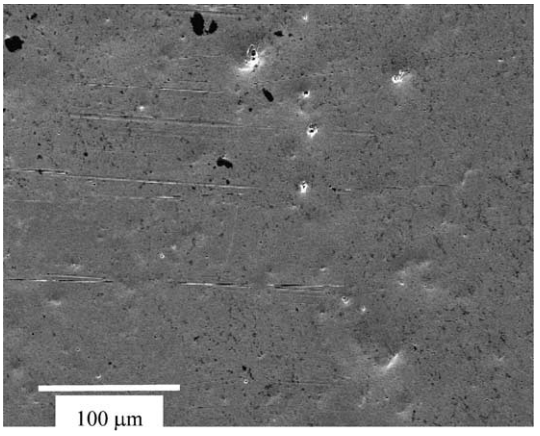

Fig. 11. Micrograph of drop test sample (upper position) after 10^3 pulses.

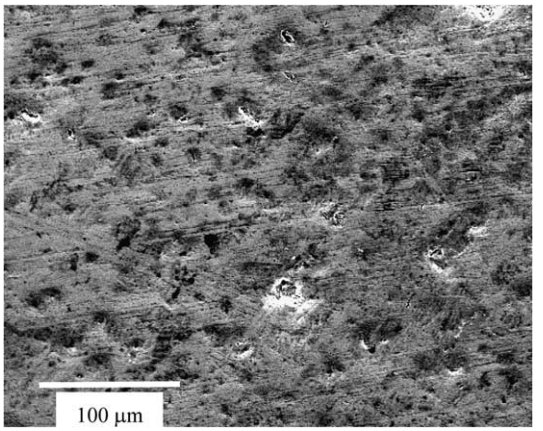

Fig. 12. Micrograph of drop test sample (upper position) after 10^4 pulses.

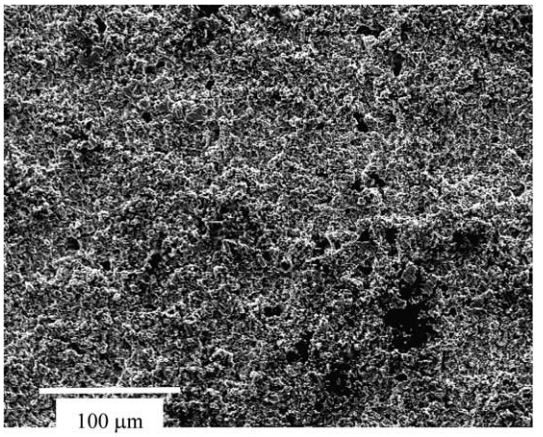

Fig. 13. Micrograph of drop test sample (upper position) after 10^5 pulses.

experienced in the beam irradiation, MIMTM, or drop test conditions. Nevertheless, the behavior of the erosion rate with number of cycles is nearly the same for this apparatus once the end of the incubation period is reached. This gives us renewed confidence in using this tool for materials screening.

Details of the tests performed recently at ORNL using an ultrasonic horn are documented in Ref. [21]. A summary of some of these recent results is shown in Fig. 14. The MDE is used as the parameter to characterize erosion in this figure and was determined using weight loss measurements. The incubation period for the ultrasonic device with annealed 316LN SS specimens is about 10^7 cycles. The incubation period is extended to about 7×10^7 cycles for the same material with 50% cold-working. Using specimens treated with the Kolsterising® process extends the incubation period slightly beyond

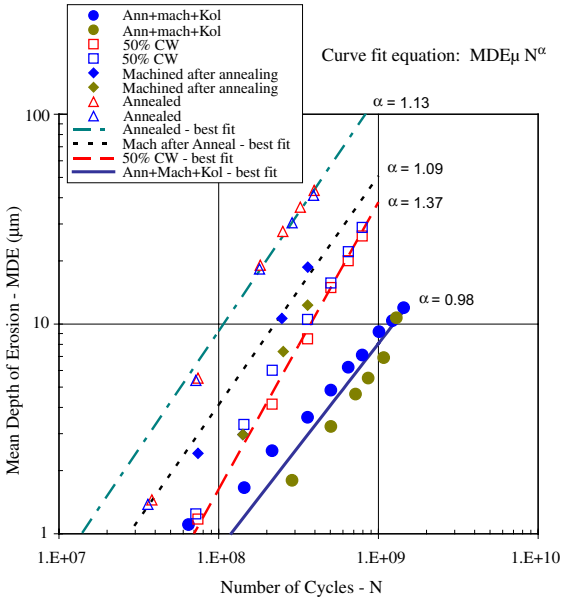

Fig. 14. Erosion data obtained using an ultrasonic horn in mercury.

that for cold-worked material. In all cases, the steady-state erosion curves appear to be well fitted by the simple relation:

$$\mathrm{MDE} = CN^{\alpha},$$

where C and α are constants, and N is the number of cycles. The values of α indicated in this figure vary from 0.98 to 1.37.

It is worth noting that cold-working 316LN SS significantly improves the cavitation erosion resistance compared with annealed material, reducing the MDE by roughly a factor of four compared with annealed material at 3×10^8 cycles. Furthermore, Kolsterising® provides a further reduction in the ultrasonic horn-induced erosion rate (roughly another factor of four beyond cold-worked material at 3×10^8 cycles) and has been shown to greatly improve the erosion resistance of welded material [21].

The apparatus that best matched beam damage on a pulse-by-pulse basis was JAERI's MIMTM device. The data obtained from this device were remarkably close to those obtained from the beam test, and the SNS team is greatly indebted to our JAERI colleagues for constructing this apparatus and gathering a considerable amount of data in a very short period of time. Futakawa has published a paper describing recent progress on understanding cavitation erosion in mercury using this device [22].

The significance of the similarity of the behavior of cavitation damage over the wide range of pressures and pulse frequencies represented by the drop test, the MIMTM device, and ultrasonic processor is remarkable and forms the basis of the extrapolation from a limited number of in-beam test pulses to the high number of pulses required for SNS. This extrapolation is discussed subsequently.

2.4. SNS erosion estimates

A summary of the in-beam and off-line cavitation damage test results is shown in Fig. 15. All results depicted in this figure use 316LN SS that has been cold worked to levels between 20% and 50%. Despite the very different pressure and frequency conditions for the three off-line tests that were operated up to a million cycles or more, they behave in a similar fashion. The damage is very low for the initial range of cycles (incubation period) and eventually becomes significant, where it follows the N^{α} relationship pointed out previously.

It appears that damage from the WNR 1.1-MW equivalent power level case is less severe than that for the MIMTM device. Therefore, the MIMTM data are assumed to represent a worst-case extrapolation of the in-beam damage. Extrapolating the MIMTM data shown in Fig. 15 leads to an MDE of less than 50 μm at 7×10^7 cycles (2 weeks operation at 60 Hz). Although the failure mechanism is not understood, this amount of erosion is judged to be acceptably small, and it is concluded that the SNS target as currently designed would

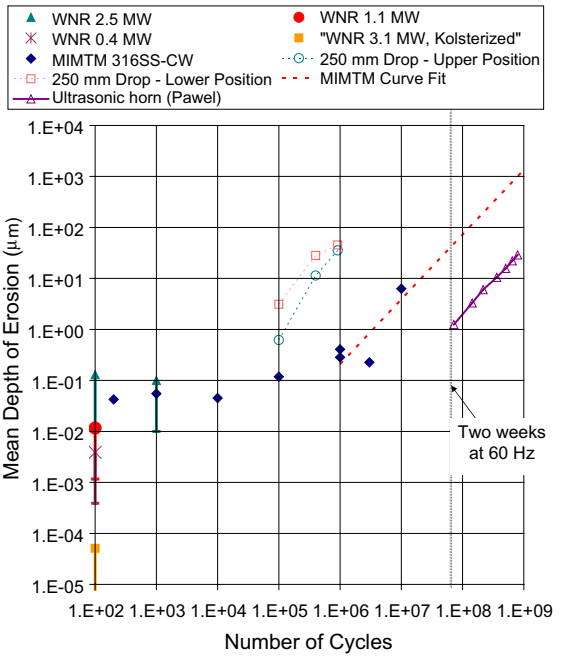

Fig. 15. Summary of mercury erosion tests.

survive two weeks of operation at an average proton beam power level of 1 MW.

3. Concluding remarks

Recent efforts aimed at quantifying the pitting damage from in-beam tests have greatly improved the understanding of this phenomenon. Results from these tests demonstrated that pitting damage is especially sensitive to beam intensity, surface treatment (Kolsterising®), and gas injection. Compared to the nominal test conditions and material surface, reducing the beam intensity by slightly more than a factor of two reduced the erosion by more than an order of magnitude, Kolsterising® the test specimen surface reduced the erosion by more than three orders of magnitude, and injecting a small amount of helium gas bubbles reduced the erosion by a factor of approximately four. Since the in-beam tests were performed for only 100–1000 beam pulses, the observed erosion is in the incubation region. These relatively large reductions in erosion are not expected to persist in the steady-state erosion region; however, these results suggest that the three parameters are likely to significantly reduce the net erosion in all cavitation regimes.

Off-line pitting simulations have been shown to cause damage with characteristics similar to those found for in-beam tests. Because these off-line tests had sufficient pressure pulse repetition rates, they were used to explore damage at high cycles. Using the results from off-line tests to scale the results from in-beam tests, it is concluded that the SNS mercury target decision criteria of achieving at least a two-week lifetime at an operating level of 1 MW has been satisfied. However, significant uncertainties and associated risks remain. Further R&D and target design efforts are needed to verify these conclusions and to extend the target to higher operating powers and longer lifetimes.

Acknowledgements

The authors wish to thank the entire SNS target R&D team for their contributions to this large effort. Obtaining the more than 6000 SEM pretest and post-test images for the in-beam experiments was a formidable task that was only made possible by the efforts of a large group of SNS engineers and scientists who volunteered over a three-month period to perform this work on nights and weekends. Special thanks are also due to our collaborators at JAERI, especially Kenji Kikuchi and Masatoshi Futakawa, who developed the MIMTM device and, along with his team, conducted many tests that were critically important to our decision-making process and provided timely analysis of the pitting damage on our drop test specimens. Special thanks also go to Forschungszentrum Jülich, especially Helmut Soltner, for conducting the bubble injection target tests, and at Los Alamos National Laboratory, especially Steve Wender, Bruce Takala, Gregg Chaparro, and Valentina Tcharnotskaia, for their help in conducting the mercury target tests at WNR. This work has benefited from the use of LANSCE at the Los Alamos National Laboratory. This facility is funded by the US Department of Energy under Contract W-7405-ENG-36.

References

[1] T.A. Gabriel, J.R. Haines, T.J. McManamy, J. Nucl. Mater. 318 (2003) 1.
[2] J.R. Haines, D.K. Felde, B.W. Riemer, C.C. Tsai, M.W. Wendel, in: Proceedings of 11th International Conference on Nuclear Engineering, Tokyo, Japan, 20–23 April 2003, ICONE11-36570.
[3] B.W. Riemer, these proceedings. doi:10.1016/j.jnucmat.2005.01.026.
[4] R.P. Taleyarkhan, F. Moraga, Nucl. Eng. Des. 207 (2001) 181.
[5] F. Moraga, R.P. Taleyarkhan, in: Proceedings of International Conference on Accelerator Applications (AccApp'99), Long Beach CA, USA, 14–18 November 1999.
[6] J. Lettry, R. Catherall, P. Drumm, A. Evensen, O. Jonsson, E. Kugler, J. Ober, J.C. Putaux, J. Sauvage, H. Ravn, M. Toulemonde, and the ISOLDE Collaboration, in: Proceedings of 13th Meeting of the International Collaboration on Advanced Neutron Sources (ICANS-XIII), Villigen, Switzerland, 11–14 October 1995.
[7] M.D. Kass, J.H. Whealton, N.E. Clapp, J.R. DiStefano, J.H. DeVan, J.R. Haines, M.A. Akerman, T.A. Gabriel, Tribol. Lett. 5 (1998) 231.
[8] M. Futakawa, H. Kogawa, R. Hino, J. Phys. IV, France 10 (2000) 247.
[9] M. Futakawa, H. Kogawa, R. Hino, H. Date, H. Takeishi, Int. J. Imp. Eng. 28 (2003) 123.
[10] K. Kikuchi, H. Kogawa, M. Futakawa, S. Ishikura, M. Kaminaga, R. Hino, J. Nucl. Mater. 318 (2003) 84.
[11] J.R. Haines, B.W. Riemer, C.C. Tsai, D.C. Lousteau, J.D. Hunn, K. Farrell, L.K. Mansur, S.A. Wender, B.E. Takala, V. Tcharnotskaia, LANSCE Activity Report 2001, LA-13943-PR, 2001.
[12] B.W. Riemer, J.R. Haines, J.D. Hunn, D.C. Lousteau, T.J. McManamy, J. Nucl. Mater. 318 (2003) 92.
[13] J.D. Hunn, B.W. Riemer, C.C. Tsai, J. Nucl. Mater. 318 (2003) 102.
[14] J.R. Price, K.W. Hylton, K.W. Tobin, P.R. Bingham, J.D. Hunn, J.R. Haines, in: Proceedings of 6th International Conference on Quality Control by Artificial Vision, 19–23 May Gatlinburg, TN, USA, 2003.
[15] J.M. Carpenter, in: Proceedings of International Workshop on Technology and Thermal Hydraulics of Heavy Liquid Metals, Schruns, Austria, 25–28 March 1996.
[16] A.E. Ruggles, 2001, private communication.
[17] M.R. Cates, D.D. Earl, Detection of Voids in Liquid Mercury During 800-MeV Proton Bombardment, Oak Ridge National Laboratory Report ORNL/TM-2002/234, 2002.

[18] M. Futakawa, in: Proceedings of 11th International Conference on Nuclear Engineering, Tokyo, Japan, 20–23 April 2003, ICONE11-36175.
[19] J.R. Haines, D.K. Felde, B.W. Riemer, C.C. Tsai, M.W. Wendel, Final Report on Mercury Target Development, SNS Project Report 101050000-TR0001, 2003.
[20] S.J. Pawel, E.T. Manneschmidt, J. Nucl. Mater. 318 (2003) 122.
[21] S.J. Pawel, these proceedings. doi:10.1016/j.jnucmat.2004.10.170.
[22] M. Futakawa, T. Naoe, H. Kogawa, C.C. Tsai, Y. Ikeda, J. Nucl. Sci. Technol. 40 (2003) 895.